SPE-184825-MS

Impact of Well Interference on Shale Oil Production Performance: A Numerical Model for Analyzing Pressure Response of Fracture Hits with Complex Geometries

Wei Yu, Texas A&M University; Yifei Xu, The University of Texas; Ruud Weijermars and Kan Wu, Texas A&M University; Kamy Sepehrnoori, The University of Texas

This paper was prepared for presentation at the SPE Hydraulic Fracturing Technology Conference and Exhibition held in The Woodlands, Texas, USA, 24-26 January 2017.

Abstract

The effect of well interference through fracture hits in shale reservoirs needs to be investigated because hydraulic fracturing is abundantly used in the development of unconventional oil and gas resources. Although numerous pressure tests have proven the existence of well interference, relatively few physical models exist to quantitatively simulate the pressure response of well interference. The objective of the present study is to develop a numerical, compositional model in combination with an embedded discrete fracture model (EDFM) to simulate well interference. Through non-neighboring connections, the EDFM can properly handle complex fracture geometries such as non-planar hydraulic fractures and a large amount of natural fractures. Based on public data for Eagle Ford shale oil, we build a reservoir model including up to three horizontal wells and five fluid pseudocomponents. The simulation results show that the connecting hydraulic fractures play a more important role than natural fractures in declining bottomhole pressure (BHP) of the shut-in well. Matrix permeability has a relatively minor impact on pressure drawdown and well productivity remains little affected due to the overall low permeability used. The BHP pressure decline profiles change from convex to concave when the conductivity of the connecting fractures increases. At early times, the BHP of the shut-in well decreases when the number of natural fractures increases. At later times, the natural fracture density has a lesser impact on the pressure response and no clear trend. The opening order of neighboring wells affects the well interference intensity between the target shut-in well with the surrounding wells. After a systematic investigation of pressure drawdown in the reservoir we formulate practical conclusions for improved production performance.

Introduction

Multi-well pads with high well density have been widely applied in the economic development of unconventional oil and gas resources. Tighter well spacing often results in the phenomenon of well-to-well interference due to fracture hits (Lawal et al. 2013; King and Valencia 2016). Such fracture hits may involve connecting both hydraulic fractures and natural fractures. Prior work has shown that the intensity of well interference increases with a decrease of well spacing (Ajani and Kelkar 2012; Kurtoglu and Salman 2015).

Similarly, infill drilling often increases the risk of fracture hits between the infill well and its neighboring wells. The fracture hits may negatively affect well performance and play an important role in optimizing well spacing to maximize overall recovery (Yaich et al. 2014; Malpani et al. 2015). Hence, minimizing the possibility of fracture hits and well interference is significant.

Field operators often utilize pressure tests to identify the intensity of well-to-well connections (Portis et al. 2013; Sardinha et al. 2014; Sani et al. 2015; Scott et al. 2015). During the pressure test process, all wells are first shut in for a certain period, then some wells are brought back on production sequentially. In the meantime, bottomhole pressure (BHP) or wellhead pressure of the shut-in well is measured and recorded (Lindner and Bello 2015). Fig. 1 presents an example of a field pressure test with observed BHP changes of shut-in Well 5 when opening Wells 1-4 sequentially in Wolfcamp shale, which clearly revealed the different degrees of well interference between Well 5 and surrounding wells (Scott et al. 2015). The physical mechanisms for inducing well interference are very complex due to the combinatory effects of matrix permeability, connecting hydraulic fractures, and natural fractures (Yu et al. 2016). However, to the best of our knowledge, the impacts of complex fracture hits such as non-planar fractures and natural fractures on pressure response of well interference have not been thoroughly studied.

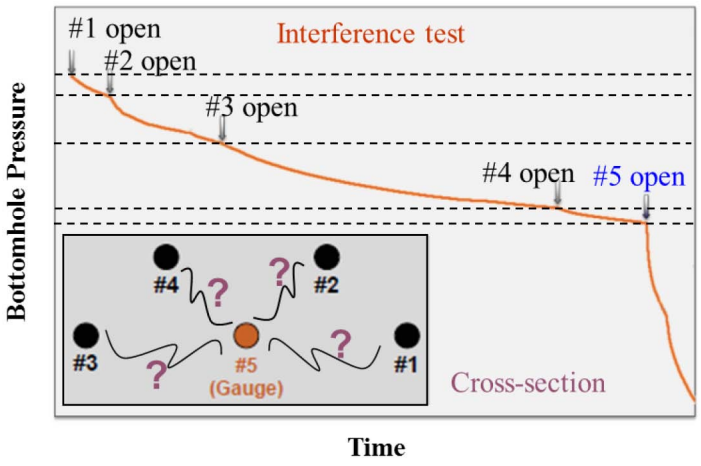

Figure 1—Example of pressure test for identifying well interference in a multi-well pad (modified from Scott et al. 2015).

Although there are many pressure test data reported in the literature to demonstrate the existence of well interference (Portis et al. 2013; Sardinha et al. 2014; Sani et al. 2015; Scott et al. 2015), few studies quantitatively simulate pressure response of well interference accounting for complex hydraulic and natural fracture geometries. Complex fracture geometries are often generated during the actual fracturing process, especially in the presence of pre-existing natural fractures (Wu et al. 2012; Cipolla and Wallace 2014; Wu and Olson 2016). The realization that such complex fracture patterns exist mandates modeling efforts should attempt to quantify their possible impact on well performance. Marongiu-Porcu et al. (2016) developed an integrated workflow through combining fracture model, reservoir simulation, and geomechanics model to reduce fracture hits and minimize interwelll fracturing interference. However, the impacts of hydraulic fracture hits and natural fractures on pressure response of the shut-in well were not captured and investigated. Awada et al. (2016) built an analytical model to simulate the pressure response of a shut-in vertically fractured well connected to another vertically fractured well through a single straight fracture hit. The impacts of matrix permeability and hydraulic fracture conductivity on pressure response were studied. However, the analytical solution is difficult to apply to multiple horizontal wells with complex fracture hits in the presence of natural fractures. Yu et al. (2016) developed a semi-analytical model to simulate the pressure response of multiple horizontal wells with complex non-planar fracture hits. The effects of connecting fracture conductivity, number of connecting fractures, and complex non-planar fracture hits

on pressure response were investigated. The semi-analytical solution cannot account for the effects of disconnected natural fractures and multiphase flow on pressure response. Hence, a new model is still needed in the petroleum industry to simulate the impacts of complex hydraulic and natural fracture geometry on pressure response of well interference.

In this study, we present the results of a numerical compositional model in combination with an embedded discrete fracture model (EDFM) capable of simulating both the pressure response to well interference and the impact on well performance. The model can incorporate complex fracture hits including non-planar hydraulic fractures and natural fractures. A basic reservoir model was developed, including two horizontal wells with multiple planar fractures. Five pseudocomponents are assumed to represent the Eagle Ford shale oil composition. We verify the model results against a commercial reservoir simulator. After verification, we investigate the impacts of different mechanisms on pressure response of well interference such as interference through matrix permeability, through connecting hydraulic fractures, and through natural fractures. In addition, we perform sensitivity studies to identify the effects of the number of connecting hydraulic fractures, conductivity of connecting hydraulic fractures, and number of natural fractures on the pressure response consequent to well interference. The basic reservoir model was expanded to include up to three horizontal wells with multiple non-planar hydraulic fractures and a large number of natural fractures. The opening order of shut-in wells during a pressure test was varied to establish which sequence best reveals the existence of fracture hits. Finally, we investigate the impact on well performance for two and three parallel horizontal wells. Our study provides a comprehensive numerical model to simulate the influence of key reservoir properties and complex hydraulic fracture geometries and natural fractures on pressure response of well interference in shale oil reservoirs.

Mathematical Formulation and Solution Procedure

The material balance equations are discretized with a finite-difference scheme using a block-centered grid. An IMPEC (implicit pressure and explicit composition) solution scheme is applied where the pressure equation is solved implicitly and the component molar balance equation is solved explicitly. Three-phase flow (water, oil, and gas) is considered for deriving the mass conservation equations for shale oil simulation in this study. The general mass conservation equation for each component can be written as

$$\frac{\partial W_i}{\partial t} + \vec{\nabla} \cdot \vec{F}_i - R_i = 0 \tag{1}$$

where t is time, W_i, $\vec{F}_i$, R_i are the accumulation, flux, and source terms, respectively (Lake et al. 1989). For component i, the terms in Eq. (1) can be expressed as

$$W_i = \phi \sum_{j=1}^{N_p} S_j \xi_j x_{ij} \tag{2}$$

$$\vec{F}_i = \sum_{j=1}^{N_p} \xi_j \vec{u}_j x_{ij} \tag{3}$$

$$\vec{u}_j = -\frac{\vec{\vec{k}} k_{rj}}{\mu_j} \left(\nabla p_j - \gamma_j \nabla D \right) \tag{4}$$

$$R_i = \frac{q_i}{V_b} \tag{5}$$

where ϕ is porosity; V_b is bulk volume; N_p refers to number of phases, which is three in our study; subscript j refers to fluid phases; S is fluid phase saturation; ξ is molar density; x is mole fraction of component in phase; $\vec{u}$ is phase velocity; $\vec{\vec{k}}$ is permeability tensor; k_r is relative permeability; μ is phase viscosity; D is depth; γ is specific gravity; p is pressure; q is molar injection or production rate.

Therefore, the overall mass conservation equation for the component i is

$$\frac{\partial}{\partial t}\left[\phi\sum_{j=1}^{N_p}S_j\xi_j x_{ij}\right]-\vec{\nabla}\cdot\left[\sum_{j=1}^{N_p}\xi_j x_{ij}\frac{\vec{\vec{k}}k_{rj}}{\mu_j}\left(\nabla p_j-\gamma_j\nabla D\right)\right]-\frac{q_i}{V_b}=0 \tag{6}$$

The equation considers fluid convection and Darcy's law. Physical dispersion and adsorption in solid phase are not considered in this study.

To solve the pressure in gridblocks, the basic assumption is that the total pore volume is the same as the total fluid volume. If we assume a slightly compressible formulation and use the chain rule, the pressure equation can be obtained as

$$\begin{aligned}&\left(V_P^0 c_f-\frac{\partial V_t}{\partial p}\right)\frac{\partial p}{\partial t}-V_b\sum_{i=1}^{N_c+1}\vec{V}_{ti}\vec{\nabla}\cdot\sum_{j=1}^{N_p}\xi_j x_{ij}\frac{\vec{\vec{k}}k_{rj}}{\mu_j}\nabla p\\&=V_b\sum_{i=1}^{N_c+1}\vec{V}_{ti}\vec{\nabla}\cdot\sum_{j=1}^{N_p}\xi_j x_{ij}\frac{\vec{\vec{k}}k_{rj}}{\mu_j}\left(\nabla p_{cj}-\gamma_j\nabla D\right)+\sum_{i=1}^{N_c+1}\vec{V}_{ti}q_i\end{aligned} \tag{7}$$

where N_c refers to number of hydrocarbon components; V_P^0 is pore volume at reference pressure; p is pressure of reference phase (oleic phase); $\vec{V}_t$ is partial molar volume; p_{cj} is capillary pressure between phase j and reference phase.

Every time step, Eq. (7) is solved implicitly to obtain the pressure at each gridblock. After that, Eq. (6) is solved explicitly to get the component moles. Saturation of each phase can be calculated by means of flash calculations (Mehra et al. 1983; Perschke et al. 1989). The fluid properties are calculated with Peng-Robinson equation of state (Lohrenz et al. 1964; Peng and Robinson 1976). This procedure is repeated until the maximum simulation time is reached.

Modeling Complex Fractures using Embedded Discrete Fracture Model

The EDFM has been shown to be an efficient method to simulate complex fracture geometries in several reservoir simulators (Moinfar et al. 2014; Shakiba and Sepehrnoori 2015; Cavalcante Filho et al. 2015; Zuloaga-Molero et al. 2016; Xu et al. 2016). In this method, fractures are discretized into small fracture segments using matrix gridblock boundaries and virtual gridblocks are created to represent these fracture segments. The flow associated with these fracture segments can be simulated inside reservoir simulators using non-neighboring connections (NNCs) or effective well indices. By keeping the structured discretization of matrix, the EDFM maintains the efficiency of structured gridding while providing a convenient way to simulate complex fractures.

In the EDFM formulations, four types of connections are considered, including the flow between matrix gridblocks and the corresponding fracture segments inside it, flow between fracture segments within an individual fracture, flow between intersecting fracture segments, and flow between fractures and well. For the first three types of connections, a general form of transmissibility factor between the NNC pair can be expressed as

$$T_{NNC} = \frac{k_{NNC} A_{NNC}}{d_{NNC}} \tag{8}$$

In Eq. (8), k_{NNC} is the permeability associated with the connection. For the matrix-fracture connection, k_{NNC} is the matrix permeability; for the fracture-fracture connection, k_{NNC} is the average fracture permeability. A_{NNC} is the contact area between the NNC pair, d_{NNC} is the distance between the NNC pair. For the matrix-fracture connection, d_{NNC} is defined as an average distance from the matrix gridblock to the fracture plane; for the fracture-fracture connection, d_{NNC} is the sum of the distances from the centroids of the fracture segments to the common line. Details of the calculation can be found in Xu et al. (2016).

Using the transmissibility factor calculated from Eq. (8), the convective terms in Eqs. (6) and (7) are modified to incorporate the NNCs. For the fracture-well connection, a modified Peaceman's model is used here to calculate the effective well index

$$WI_f = \frac{2\pi k_f w_f}{\ln(r_e / r_w)} \tag{9}$$

$$r_e = 0.14\sqrt{L^2 + W^2} \tag{10}$$

where w_f is the fracture aperture, k_f is the fracture permeability, L is the length of the fracture segment, and W is the height of the fracture segment.

Using the EDFM approach, a large number of fractures can be conveniently modeled in our simulator without using unstructured gridding. The connections in the EDFM are implemented as non-neighboring connections inside the simulator. In this study of well interference, the connectivity between fractures are appropriately captured and simulated by the EDFM.

Model Verification

A synthetic shale-oil case was built based on publicly available Eagle Ford data in order to verify the new developed numerical model (Orangi et al. 2011; Simpson et al. 2016). Fluid types in the Eagle Ford range from black oils with low gas oil ratio (GOR) to volatile oils with high GOR (Orangi et al. 2011). In our study, black oil with low GOR is considered. Fluid characterization data for Eagle Ford shale is scarce in literature. In our study we assume crude oil of the Eagle Ford formation consists of five pseudocomponents, i.e., CO_2, N_2-C_1, C_2-C_5, C_6-C_{10}, and C_{11+}. The corresponding molar fractions are 0.01821, 0.44626, 0.17882, 0.14843, and 0.20828, respectively. According to the critical properties of these pseudocomponents and the other inputs in the Tables 1 and 2, the key oil properties were determined using the Peng-Robinson equation of state and flash calculations under the reservoir temperature of 270 °F: oil gravity is 41 °API, GOR is 1,000 scf/stb, formation volume factor is 1.65 rb/stb, and bubble point is 3,446 psi, which are the same as the data reported by Orangi et al. (2011).

Table 1—Compositional data for the Peng-Robinson equation of state in the Eagle Ford formation.

Component	Molar fraction	Critical pressure (atm)	Critical temperature (K)	Critical volume (L/mol)	Molar weight (g/gmol)	Acentric factor	Parachor coefficient
CO_2	0.01821	72.80	304.20	0.0940	44.01	0.2250	78.00
N_2-C_1	0.44626	45.24	189.67	0.0989	16.21	0.0084	76.50
C_2-C_5	0.17882	32.17	341.74	0.2293	52.02	0.1723	171.07
C_6-C_{10}	0.14843	24.51	488.58	0.3943	103.01	0.2839	297.42
C_{11+}	0.20828	15.12	865.00	0.8870	304.39	0.6716	661.45

Table 2—Binary interaction parameters for oil components in the Eagle Ford formation.

Component	CO_2	N_2-C_1	C_2-C_5	C_6-C_{10}	C_{11+}
CO_2	0	0.1036	0.1213	0.1440	0.1500
N_2-C_1	0.1036	0	0	0	0
C_2-C_5	0.1213	0	0	0	0
C_6-C_{10}	0.1440	0	0	0	0
C_{11+}	0.1500	0	0	0	0

We set up a basic reservoir model with length, width, and thickness of 6,550 ft × 2,150 ft × 100 ft, which corresponds to reservoir dimensions shown in Fig. 2. Two horizontal wells with multiple planar hydraulic fractures are modeled first. The separation of the two wells is 700 ft and each well contains 30 transverse hydraulic fractures with fracture half-length of 225 ft. The EDFM method is applied to model hydraulic fractures which does not require any local grid refinement (LGR). LGR was still needed to account for the hydraulic fractures in the numerical reservoir simulator, in order to fully capture the transient flow behavior of fluid transfer from the matrix to fractures (Yu et al. 2016). The basic reservoir and fracture properties used in the simulations are listed in Table 3.

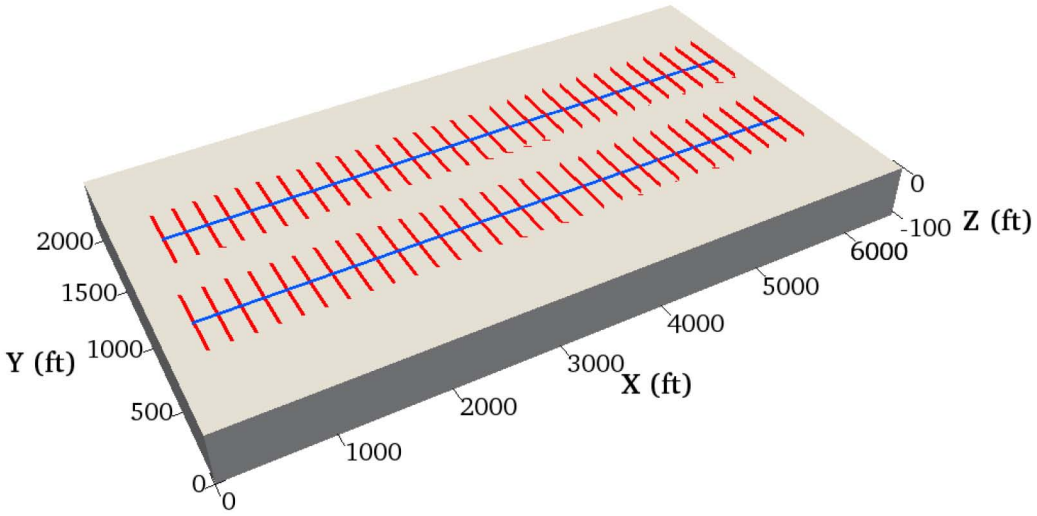

Figure 2—A basic reservoir model including 2 horizontal wells (blue lines) each with 30 planar hydraulic fractures (red lines).

Table 3—Basic reservoir and fracture properties used for the simulations.

Parameter	Value	Unit
Initial reservoir pressure	8,000	psi
Reservoir temperature	270	°F
Reservoir permeability	470	nD
Reservoir porosity	12%	-
Initial water saturation	17%	-
Total compressibility	3×10^{-6}	psi^{-1}
Fracture half-length	225	ft
Fracture conductivity	100	md-ft
Fracture height	100	ft
Fracture width	0.01	ft
Fracture spacing	200	ft
Well spacing	700	ft

A constant flowing initial BHP of 2,000 psi is assumed for each well at the start of the simulations. Hydraulic fractures are assumed to fully penetrate the reservoir thickness. The assumed relative permeability curves, such as water-oil relative permeability and liquid-gas relative permeability, are given in Fig. 3. The comparison of gas and oil flow rates between this model and numerical reservoir simulator (CMG 2012) is shown in Fig. 4, illustrating that good agreement was obtained. The pseudocomponents for shale oil adopted in our model ensure fluid properties (density, viscosity, and composition) correspond to values under reservoir condition at all times. The formation volume factor follows from the ratio of fluid volume at surface and under reservoir conditions, as is GOR, both of which are obtained from the pseudocomponents flash calculations in the results of Fig. 4.

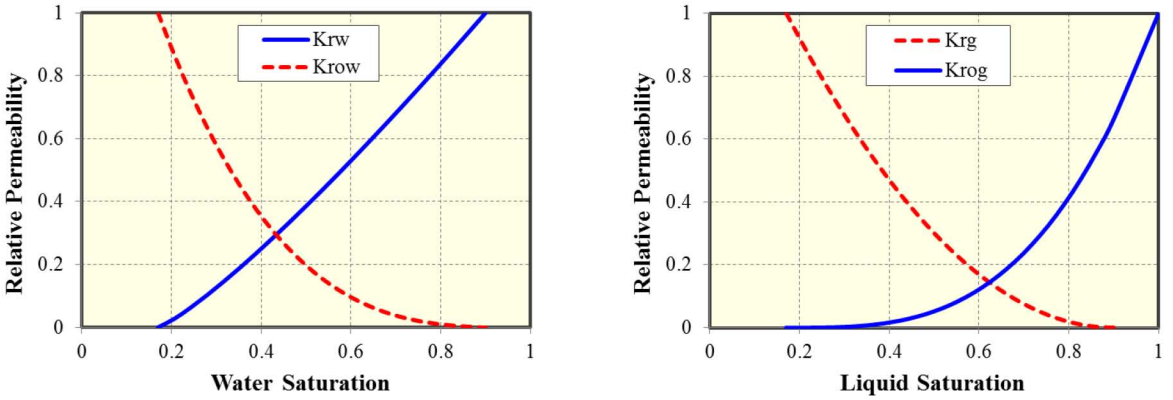

(a) Water-oil relative permeability curve (b) Liquid-gas relative permeability curve

Figure 3—Relative permeability curves used in this study.

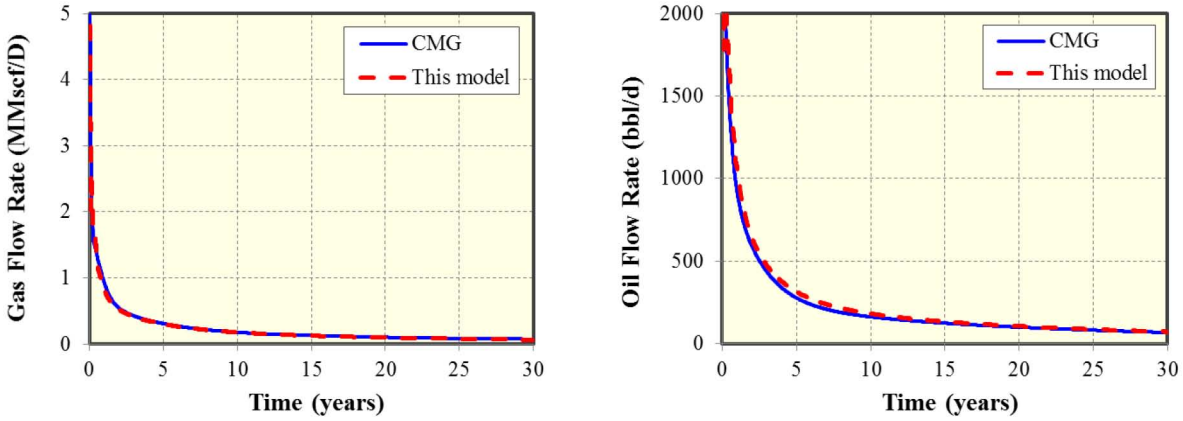

(a) Gas flow rate (b) Oil flow rate

Figure 4—Comparison of well performance between this model and numerical reservoir simulator.

Case Studies

Four cases

In order to examine the impacts of different physical mechanisms such as matrix permeability, hydraulic fracture hits and natural fractures on pressure response of well interference, we designed four cases, each comprised of two parallel horizontal wells, but with different degrees of fracture density (and connectivity), as illustrated in Fig. 5. *Case 1* represents well interference through matrix permeability with neither any natural fractures nor any connecting hydraulic fractures. *Case 2* represents well interference through both the matrix permeability and via natural fractures partly connected to the regular set of hydraulic fractures. The natural fractures occur in two dominant orientations and the total number of natural fractures is 1,000 in the reservoir volume studied (black lines). More specifically, a statistical method was used to generate the natural fracture sets. The angle with respect to the x axis for one set ranges from 5 to 25 degree and the other set ranges from 95 to 115 degree. The length of the natural fractures varies between 100 ft and 300 ft. The conductivity of the natural fractures is fixed at 1 md-ft. The natural fracture height in our model is assumed equal to the reservoir thickness. *Case 3* represents well interference through both matrix permeability and via hydraulic fracture hits, but without any natural fractures. The two wells are interconnected via five hydraulic fracture hits each with fracture conductivity of 100 md-ft. *Case 4* represents well interference through the combination of matrix permeability, natural fractures and connecting hydraulic fractures. The other reservoir and fracture properties remain the same as those in Tables 1-3. The simulation time is 1,000 days. The upper horizontal well is producing under the constant BHP of 2,000 psi while the lower horizontal well remains shut-in at all times.

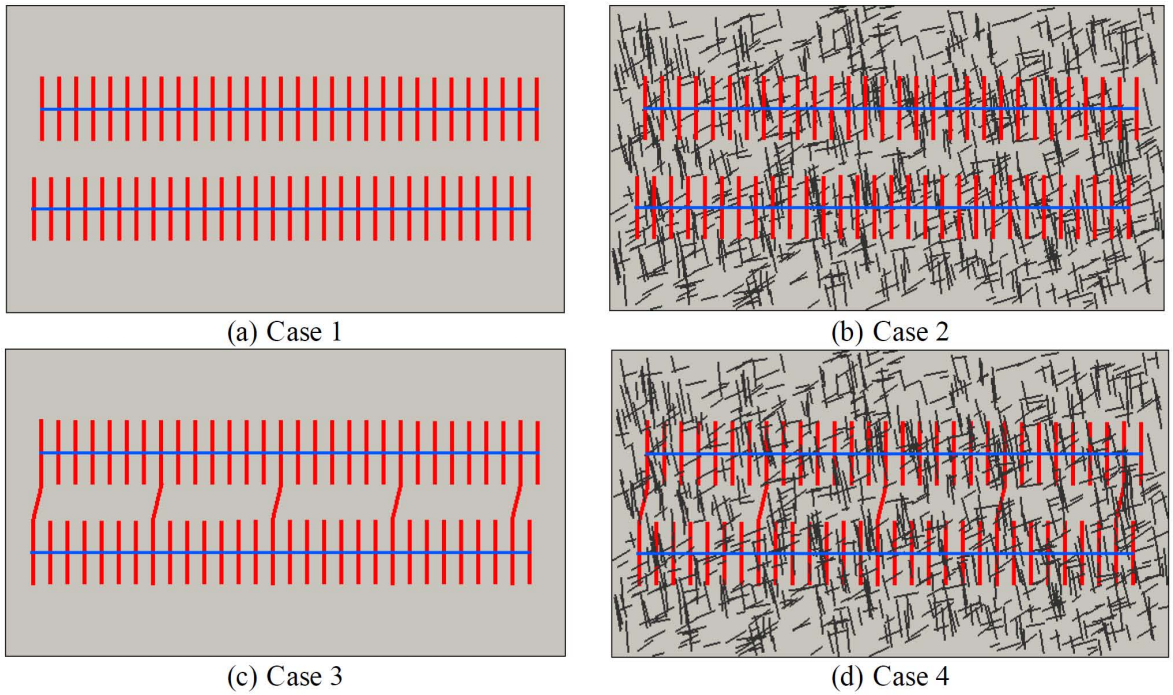

Figure 5—Map view of four cases demonstrating the different mechanisms inducing well interference such as matrix permeability, hydraulic fracture hits, natural fractures, and the combination of them.

The pressure response of the shut-in well and cumulative oil production of the producing well for each of the four cases is presented in Fig. 6. For *Case 1*, the effect of matrix permeability on BHP decline of the shut-in well within 1,000 days is negligible due to the low matrix permeability of 470 nD and assuming an otherwise constant porosity for all cases. For *Case 2*, the BHP decline is small at early times and subsequently decreases almost linearly at later times. For *Case 3*, the BHP declines relatively fast at early times but then the decline rate slows at later times. Comparing *Cases 2* and *3* indicates that the connectivity via hydraulic fracture hits in our model is more important for well interference than the effect of natural fractures. For *Case 4*, the BHP declines at early times slower than for *Case 3* but then faster at later times. For *Case 4*, oil production from natural fractures likely helps sustain productivity of the open well. Fig. 6(b) confirms that the presence of natural fractures (*Cases 2* and *4*) significantly boosts the performance of the producing well.

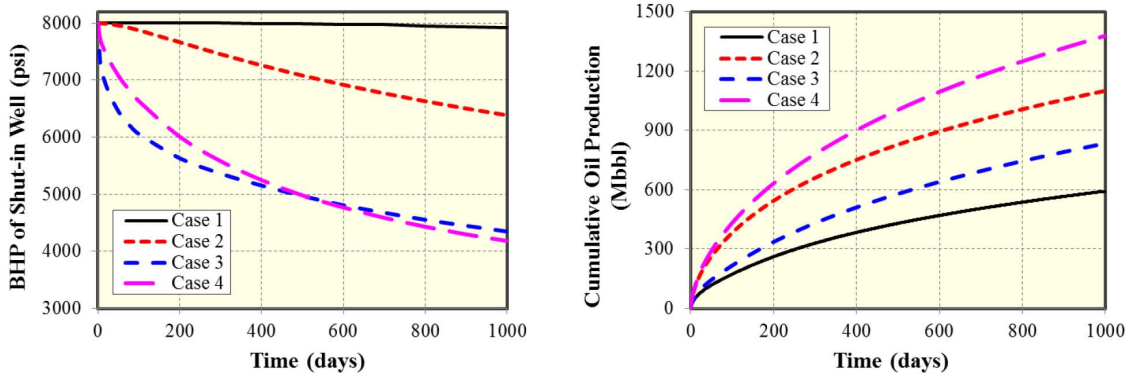

(a) BHP of the shut-in well (b) Cumulative oil production

Figure 6—Comparison for four cases of (a) pressure response of the shut-in lower well after opening upper well and (b) cumulative oil production of the producing well.

Fig. 7 shows the pressure distribution in the reservoir for each case after 1,000 days of production. For *Case 1* [Fig. 7(a)], well interference is absent and reservoir depletion around the shut-in well cannot occur. When well interference occurs due to the existence of natural fractures as in *Case 2* [Fig. 7(b)], the drainage area of the producing well becomes somewhat enhanced as compared to *Case 1*. Fluid flows from the shut-in well to the producing well via some connected natural fractures. Since the conductivity of the connecting natural fractures is very small (1 md-ft) any reservoir depletion around the shut-in well remains negligible. When well interference increases due to connection of the two wells by hydraulic fracture hits as in *Case 3* [Fig. 7(c)], fluid flows faster from the shut-in well to the producing well, aided by larger conductivity of the connecting hydraulic fractures, resulting in some discernable drainage around the shut-in well. When well interference occurs due to a combination of effects as in *Case 4* [Fig. 7(d)], the drainage area encompasses both the producing well and the shut-in well, and consequent reservoir depletion area is largest.

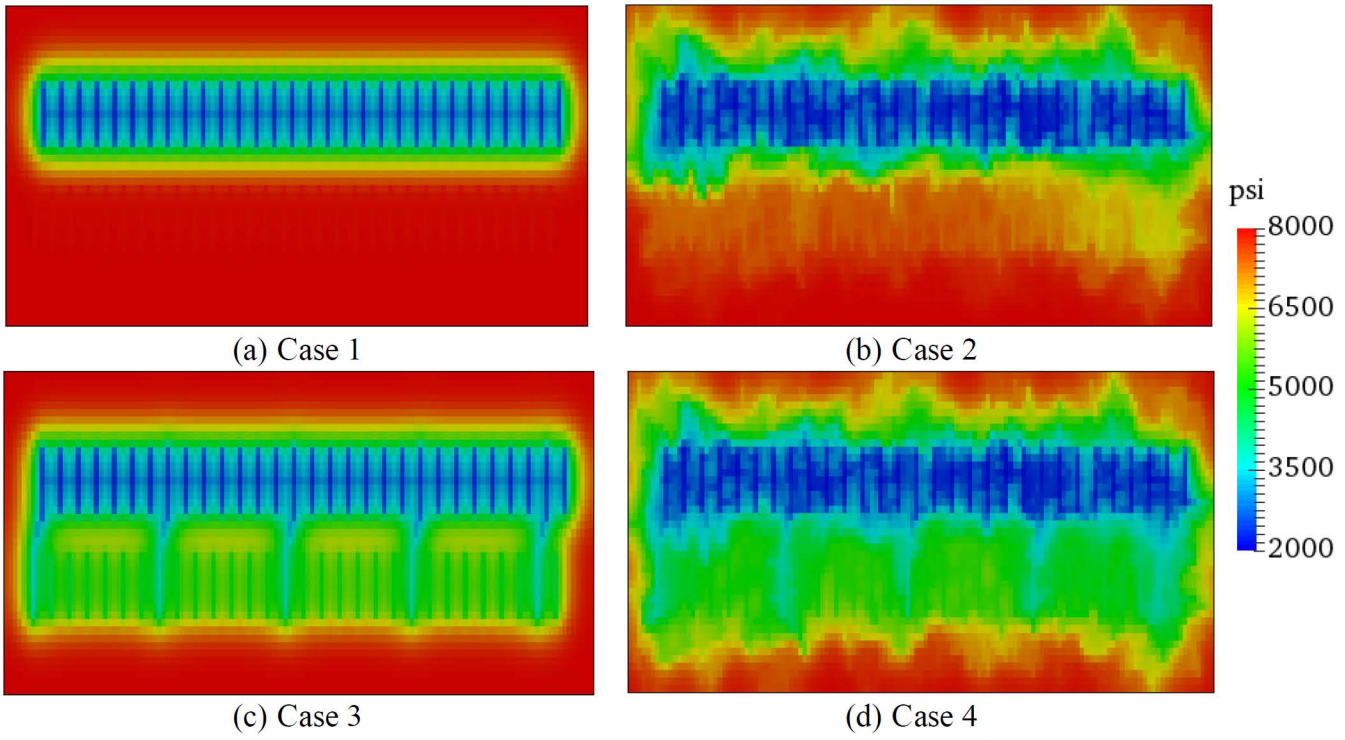

Figure 7—Comparison of pressure distribution between four cases after 1,000 days of production.

Sensitivity Analysis

Effect of connecting fracture conductivity

On the basis of *Case 3* with five fracture hits, we investigated the impact on pressure response of four discrete cases with different conductivity for the set of fracture hits, namely 0.1, 1, 10 and 100 md-ft, as shown in Fig. 8. The BHP of the shut-in well decreases most rapidly when the conductivity of the connecting fractures is higher. In addition, the profile of BHP decline changes from convex to concave with an increase in fracture conductivity. The BHP result for the low fracture conductivity (0.1 md-ft) suggests that the pressure response of well interference is difficult to identify at early times of production even though there are multiple hydraulic fracture hits. Fig. 8(b) graphs the cumulative oil production for the upper, open well for each set of fracture hit conductivities. As to be expected, cumulative production increases with increasing conductivity of the connecting fractures. The reservoir pressure distribution after 1,000 days of production is shown in Fig. 9 for each fracture hit conductivity.Fluids flow faster from the shut-in well to the producing well when the conductivity of the connecting fractures is higher, as can be physically expected.

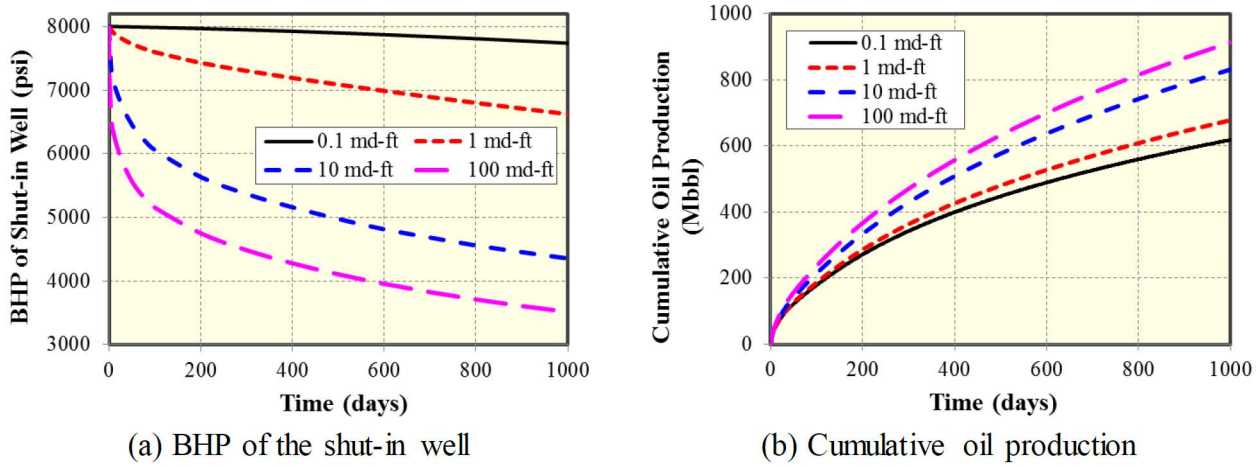

(a) BHP of the shut-in well (b) Cumulative oil production

Figure 8—Effect of connecting fracture conductivity on pressure response of the shut-in well and cumulative oil production of the producing well.

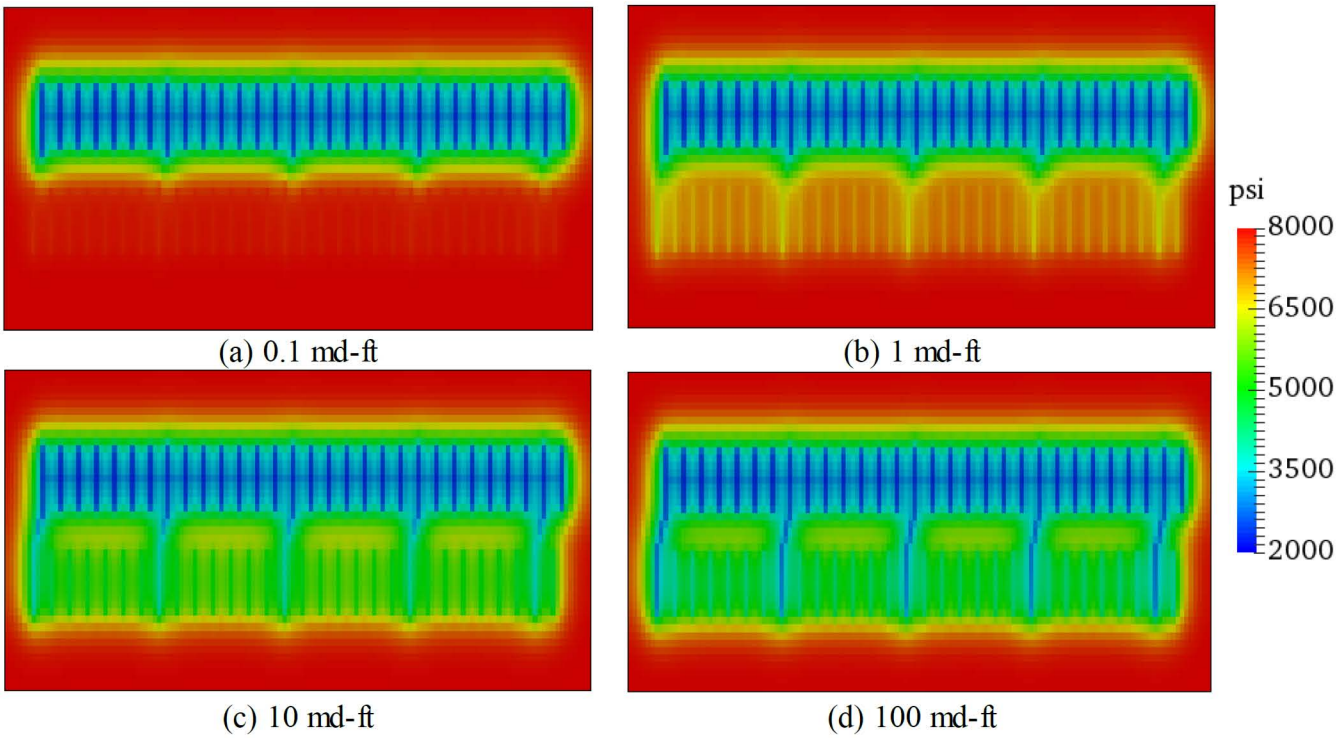

(a) 0.1 md-ft (b) 1 md-ft

(c) 10 md-ft (d) 100 md-ft

Figure 9—Comparison of pressure distribution under different connecting fracture conductivities after 1,000 days of production.

Effect of number of connecting hydraulic fractures

We separately investigated the impact on pressure response for a discrete number of fracture hits, referring to the number of hydraulic fractures connecting the well pair, comparing the effect of 3, 5, 8 and 15 hits, as shown in Fig. 10. The conductivity of all fracture hits was kept constant at 100 md-ft. The resulting BHP of the shut-in well and the cumulative oil production of the open well for each case is shown in Fig. 11. The BHP of the shut-in well decreases faster when the fracture hits increase, confirming that the number of connecting fractures plays an important role in pressure response of well interference. Similarly, cumulative oil production of the open well increases when the number of connecting hydraulic fractures increases. The pressure distribution pattern in the reservoir after 1,000 days of production for each case is shown in Fig. 12. These pressure images clearly demonstrate that fluid migrates faster away from the shut-

in well to the producing well when the number of connecting hydraulic fractures increases. Depletion of the reservoir section drained by the well pair benefits from fracture hits, when one well is kept shut-in. However, simultaneous production by keeping both wells under production will certainly be faster, but requires a double set of pumps and separators, offsetting some of the net present value gains due to faster production.

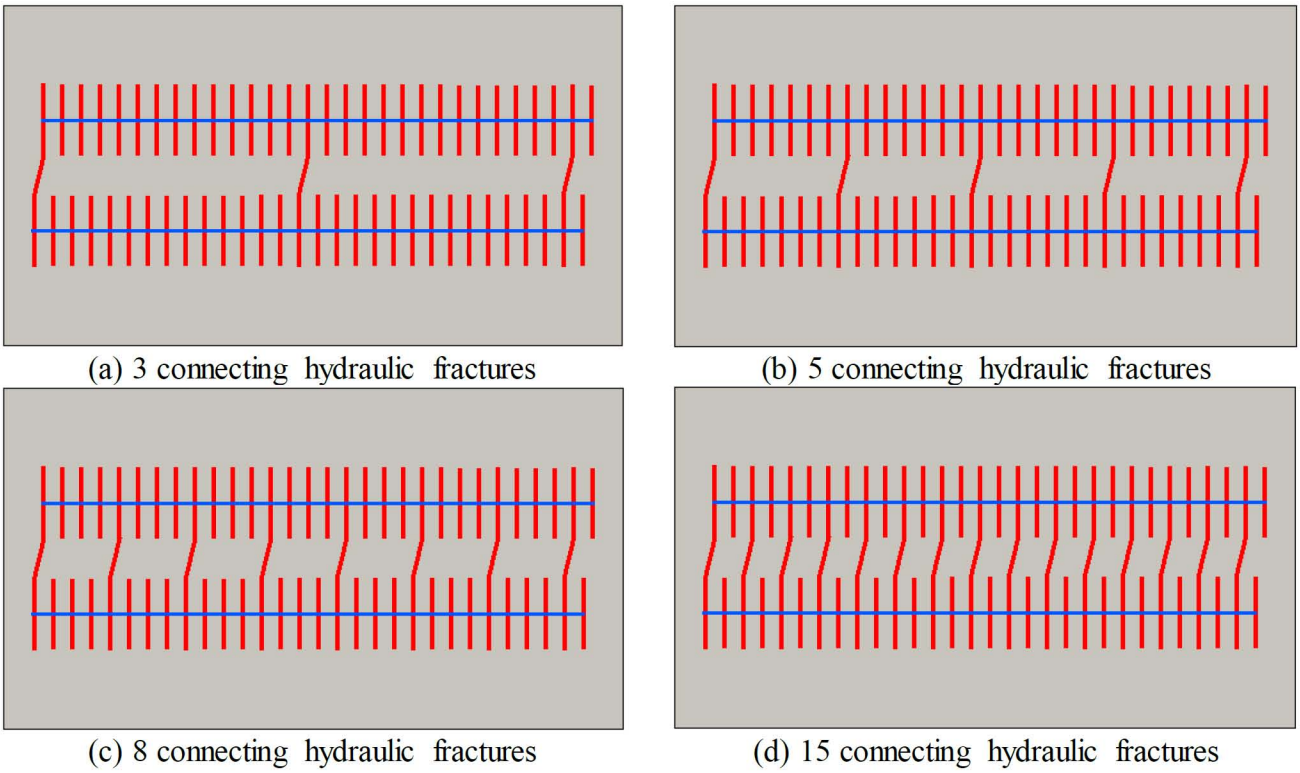

Figure 10—Map view of different number of connecting hydraulic fractures inducing well interference.

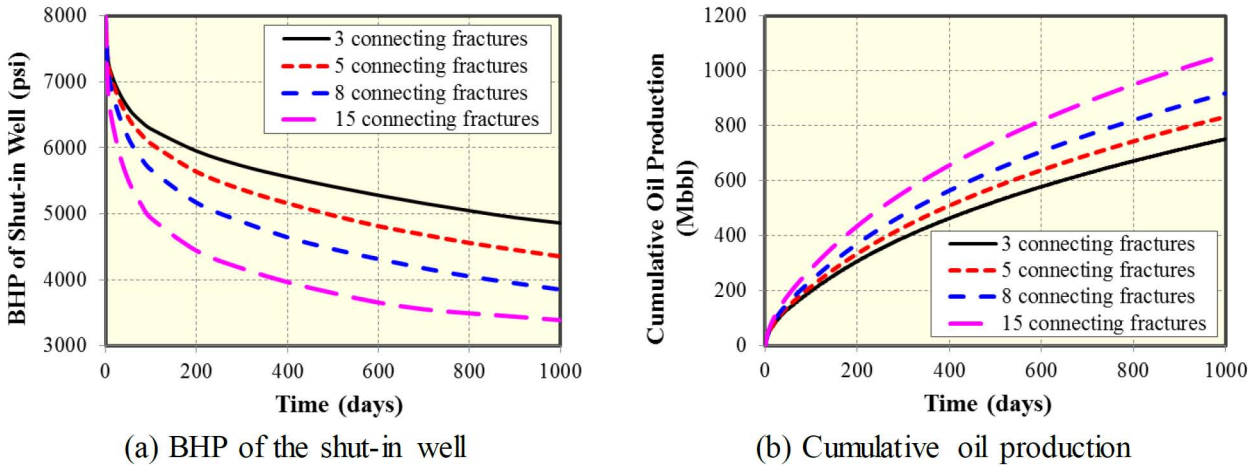

Figure 11—Effect of number of connecting hydraulic fractures on pressure response of the shut-in well and cumulative oil production of the producing well.

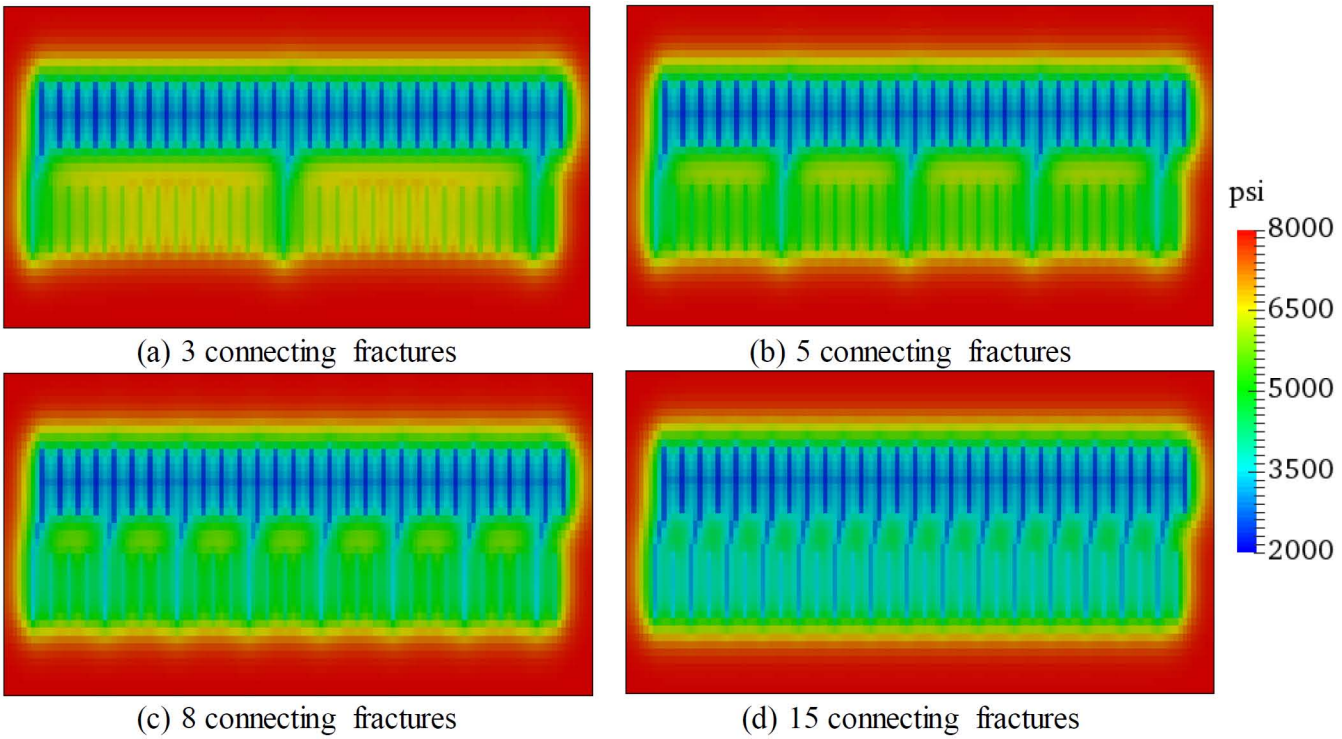

Figure 12—Comparison of pressure distribution under different number of connecting hydraulic fractures after 1,000 days of production.

Effect of number of natural fractures

We investigated the impact on pressure response and well productivity for four discrete cases with different natural fracture density, namely 100, 500, 1,000 and 1,500 fractures per study area volume, as shown in Fig. 13. The natural fracture parameters such as natural fracture length, angle, and height remain the same as in *Case 4* [Fig. 5(d)]. The resulting impacts on BHP of the shut-in well and the cumulative oil production of the producing well are shown in Figs. 14**(a)** and **(b)**, respectively. The BHP of the shut-in well consistently decreases faster at early flow times when natural fracture density increases. However, the pressure decline rate is inconsistent at later times, which we attribute to detailed interference effects connected to natural fracture location and variations in degree of connectivity between natural fractures and hydraulic fractures. More efforts will be made in future studies to explain in detail why the change in pressure response varies over time when natural fractures and hydraulic fractures interfere. The cumulative oil production of the open well consistently increases when the natural fracture density increases [Fig. 14(b)]. The reason is that overall drainage by fractures (both hydraulic and natural) is more effective for higher density of natural fractures.

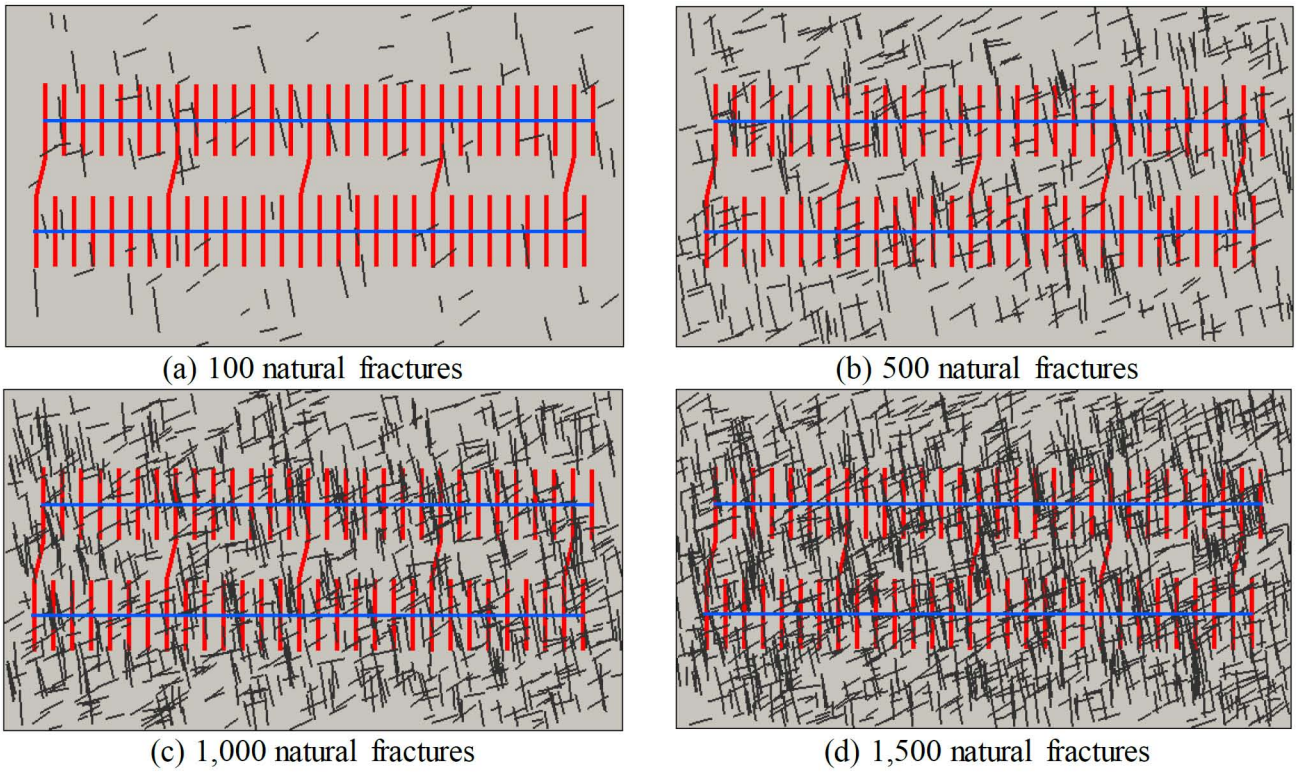

Figure 13—Map view of different number of natural fractures inducing well interference.

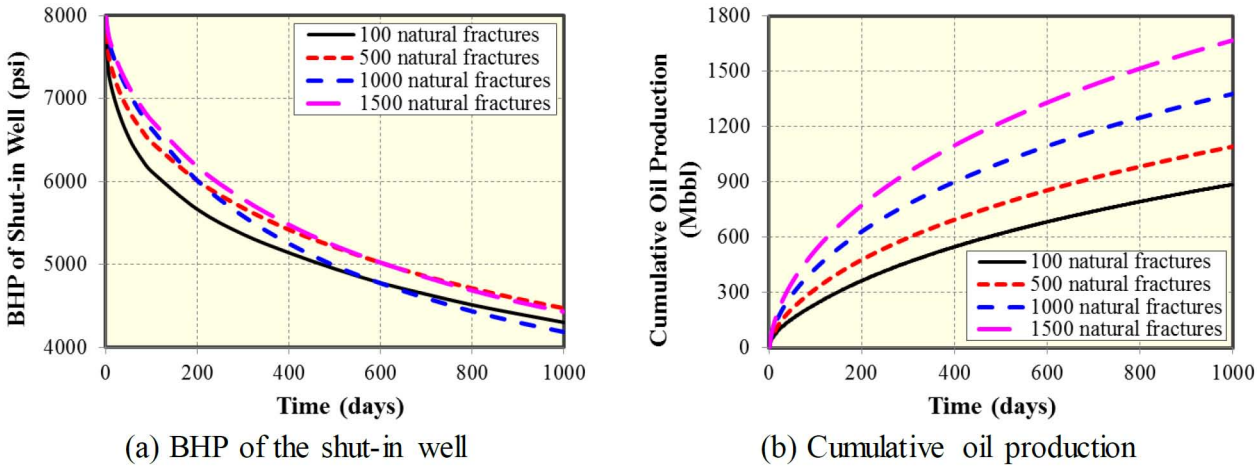

Figure 14—Effect of number of natural fractures on pressure response of the shut-in well and cumulative oil production of the producing well.

A comparison of pressure distributions after 100 days of production is shown in Figs. 15**(a)-(d)** for various densities of natural fractures. These results reveal that the drainage area of the producing well increases when the number of natural fractures increases. The more advanced pressure drawdown pattern after 1,000 days of production is shown in Fig. 16. Even for such longer production times, the drainage area of the producing well is consistently the larger when natural fractures are more abundant.

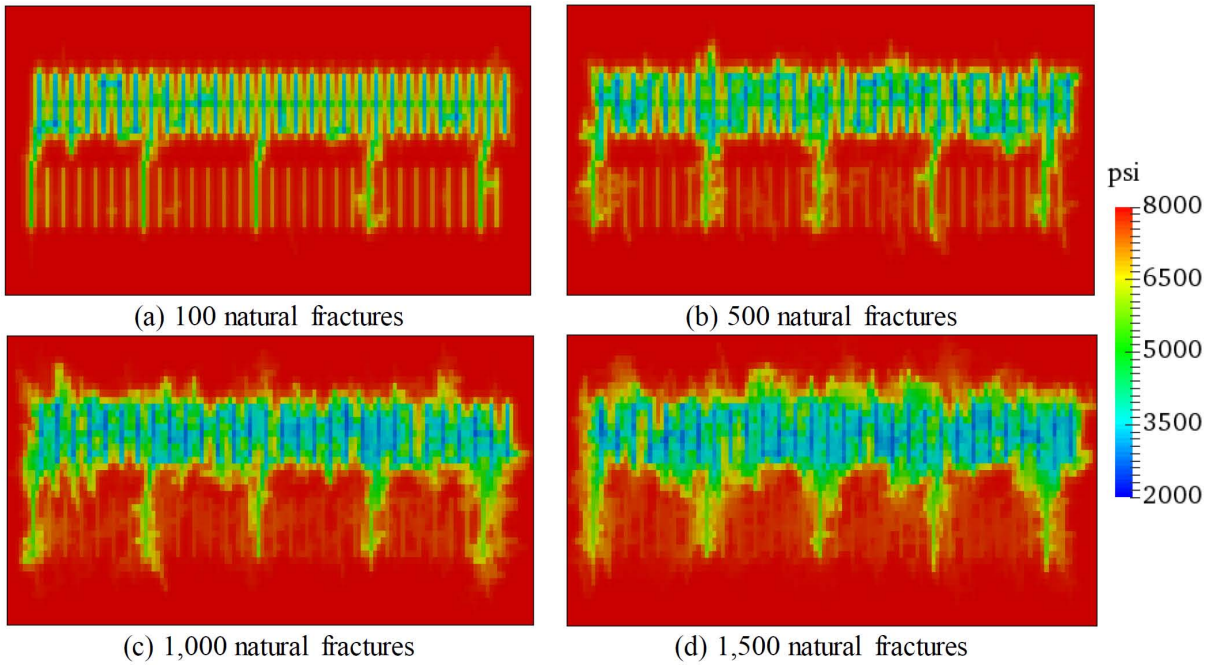

Figure 15—Comparison of pressure distribution under different number of natural fractures after 100 days of production.

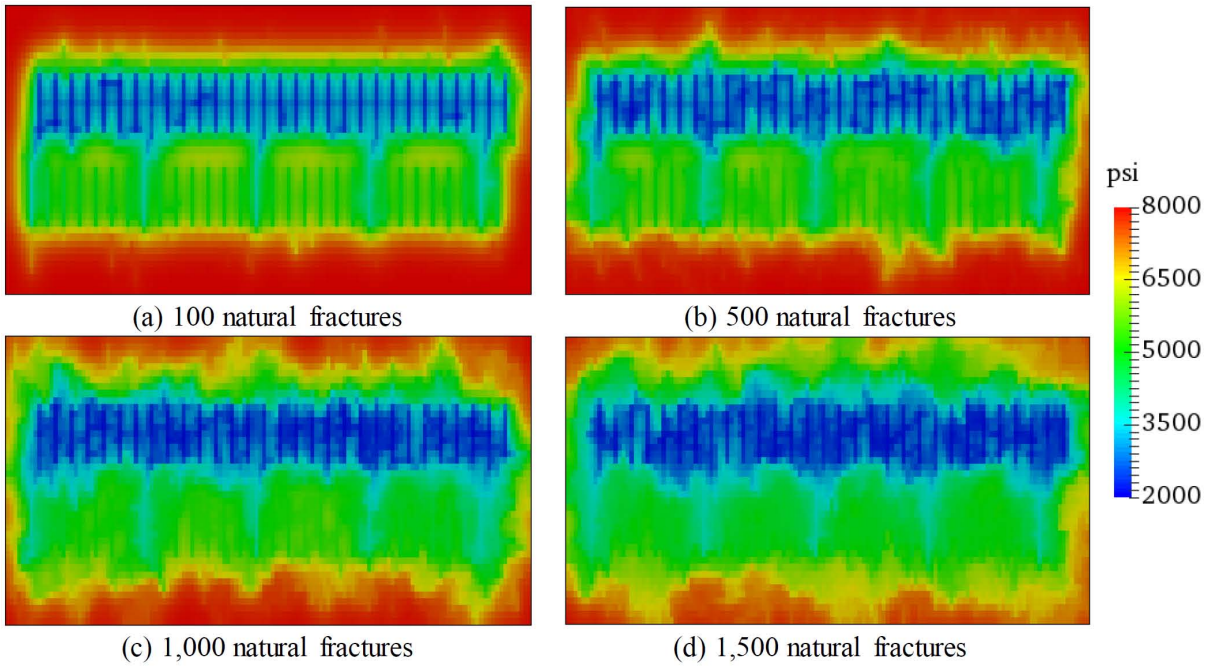

Figure 16—Comparison of pressure distribution under different number of natural fractures after 1,000 days of production.

Well Shut-in Test Simulation

Simulation of different well interference intensity of three wells

In order to examine the different well interference intensity between the target well and its surrounding wells, we expanded the width of the above basic reservoir model to 2,850 ft, in order to accommodate three horizontal wells, as shown in Fig. 17. The distance between two neighboring wells is still 700 ft and each well has 30 non-planar hydraulic fractures. Additionally, the model includes 2,000 natural fractures and their parameter settings such as fracture length, angle, and height are similar as before. The simulation

time is 100 days. The middle well is always shut-in. We designed two scenarios for the other two wells to identify well interference effects on well productivity. *Scenario 1*: the upper well first opens to produce for one month, then the lower well opens to produce. *Scenario 2*: the lower well first opens to produce for one month, then the upper well is also opened to produce.

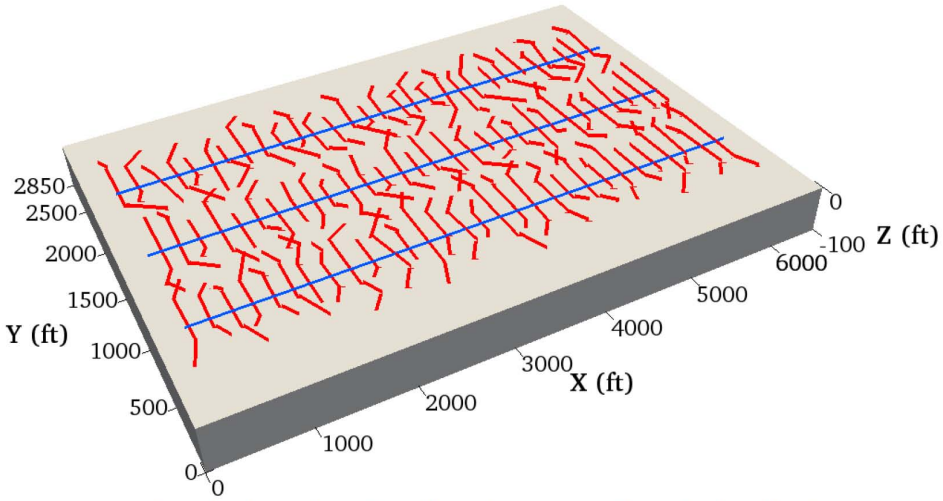

(a) Three horizontal wells with only 90 non-planar hydraulic fractures

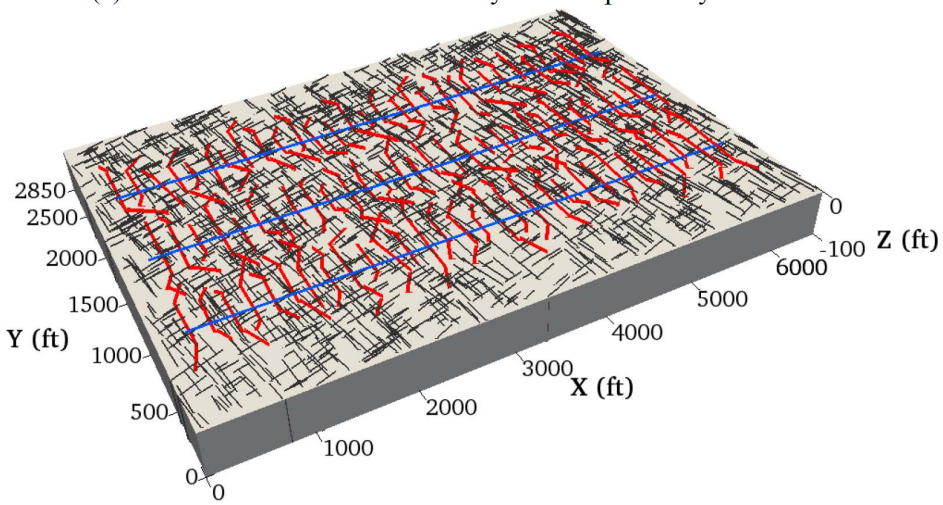

(b) Three horizontal wells with 90 non-planar hydraulic fractures and 2,000 natural fractures

Figure 17—The extended basic reservoir model including three horizontal wells, multiple non-planar hydraulic fractures and natural fractures.

Fig. 18 compares the BHP decline behavior for each of the two scenarios. For *Scenario 1*, the BHP of the shut-in well decreases slowly when the upper well opens first. However, the BHP rapidly declines when the lower well is also opened to produce after 30 days. The lower well has a much stronger well interference with the middle well than the upper well. For *Scenario 2*, the BHP of the shut-in well decreases quickly when the lower well opens first and there is a slower, but continuous decline after 30 days when the upper is additionally opened to produce. The upper well has a smaller well interference with the middle well as compared to the lower well. Hence, the scenario 1 performs better than the scenario 2 to identify the well interference intensity between the middle well with its neighboring wells. Fig. 19 compares the pressure distribution pattern of the two scenarios after 30 days prior to opening of the other well. The well interference between the middle well and lower well is larger than the well interference between the middle and the upper well.

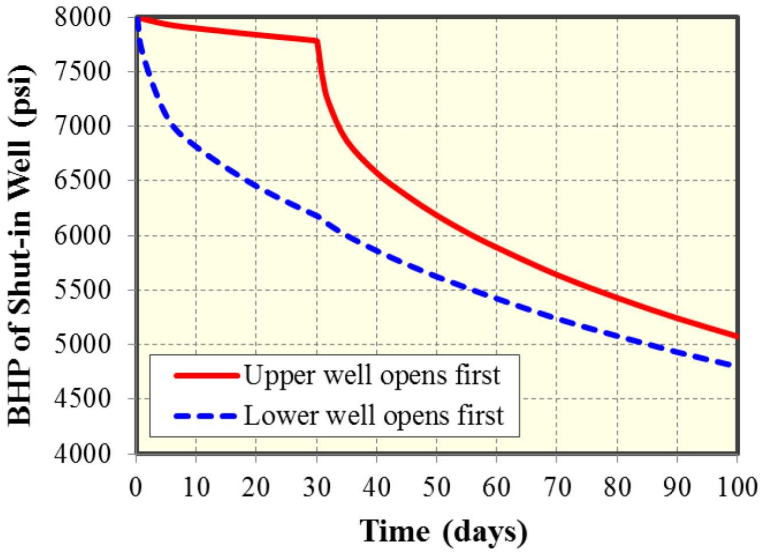

Figure 18—Comparison of BHP decline behavior of the shut-in well for two different scenarios.

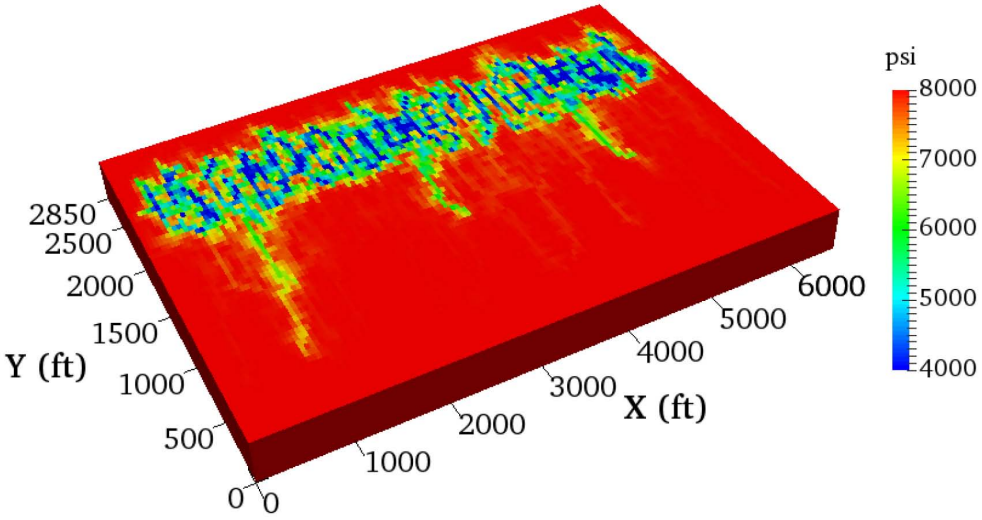

(a) Scenario 1

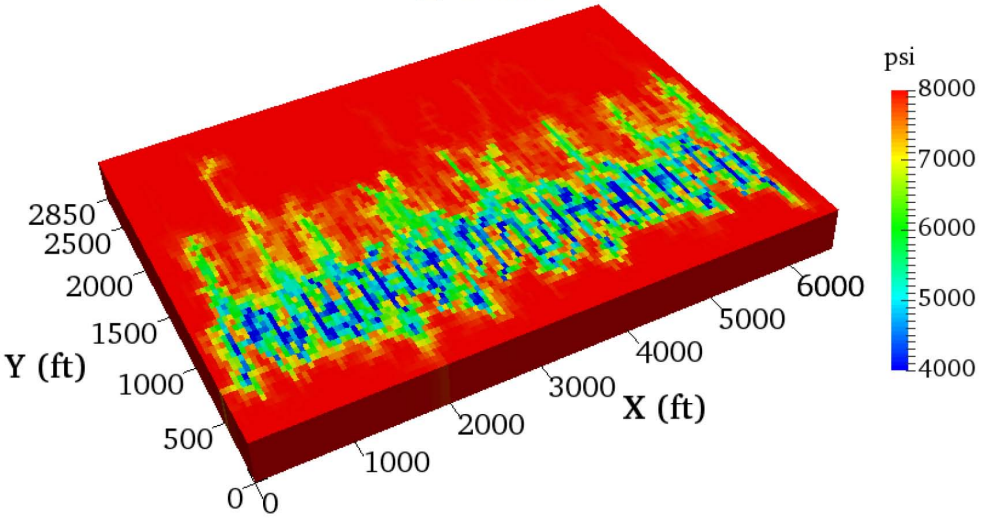

(b) Scenario 2

Figure 19—Comparison of pressure distribution between two different scenarios after 100 days of production.

Well Spacing Effects

All wells open

Next, we simulated the reservoir depletion effectiveness by varying well spacing in the study area from one well (*Case 1*) to 2 wells (*Case 2*) to 3 parallel horizontal wells (*Case 3*) (Fig. 20). The location and density of natural fractures remains the same for each case (Fig. 17). Fig. 21 presents a comparison of the cumulative oil and gas production for each of the three cases over a 30-year production period. Total production of the region after 30 years with one well is only 51% and with two wells 96% as compared to production from three wells. A full economic analysis to determine the optimal number of wells was not conducted in our study, but if three wells only produce 4% more oil over 30 years, two horizontal wells (1,400 ft apart) for our study area are a better well spacing than three wells (700 ft apart). Fig. 22 shows the reservoir pressure distribution for each case after 1,000 days of production. Although after 1,000 days (2.7 years) the pressure distribution suggests much better drainage for 3 wells, ultimate production of three open wells (none shut-in) after 30 years is only 4% larger as compared to production with two open wells (none shut-in) [Fig. 21(b)].

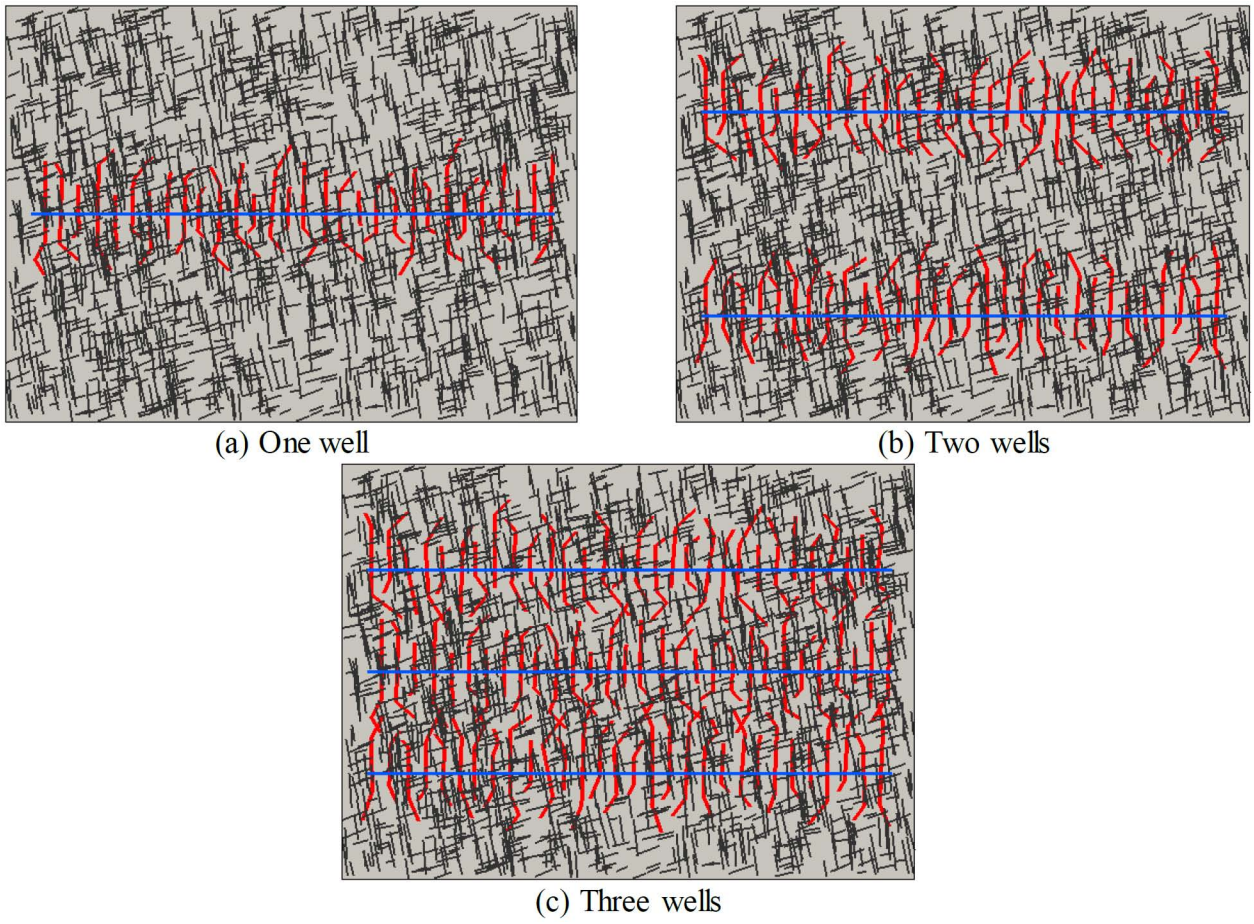

Figure 20—Three cases with different number of horizontal well.

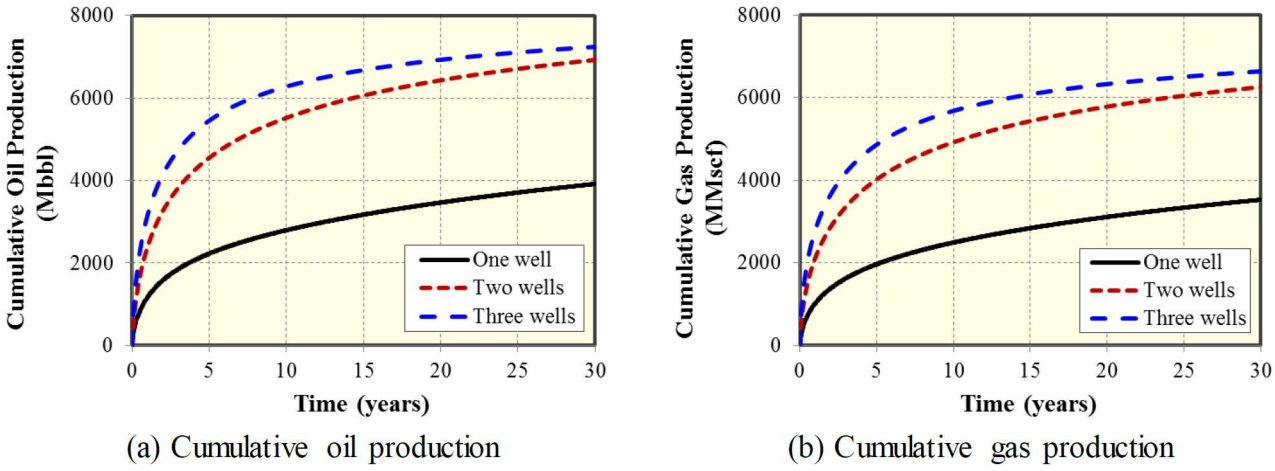

Figure 21—Comparison of well performance between three cases with different well number at 30 years of production.

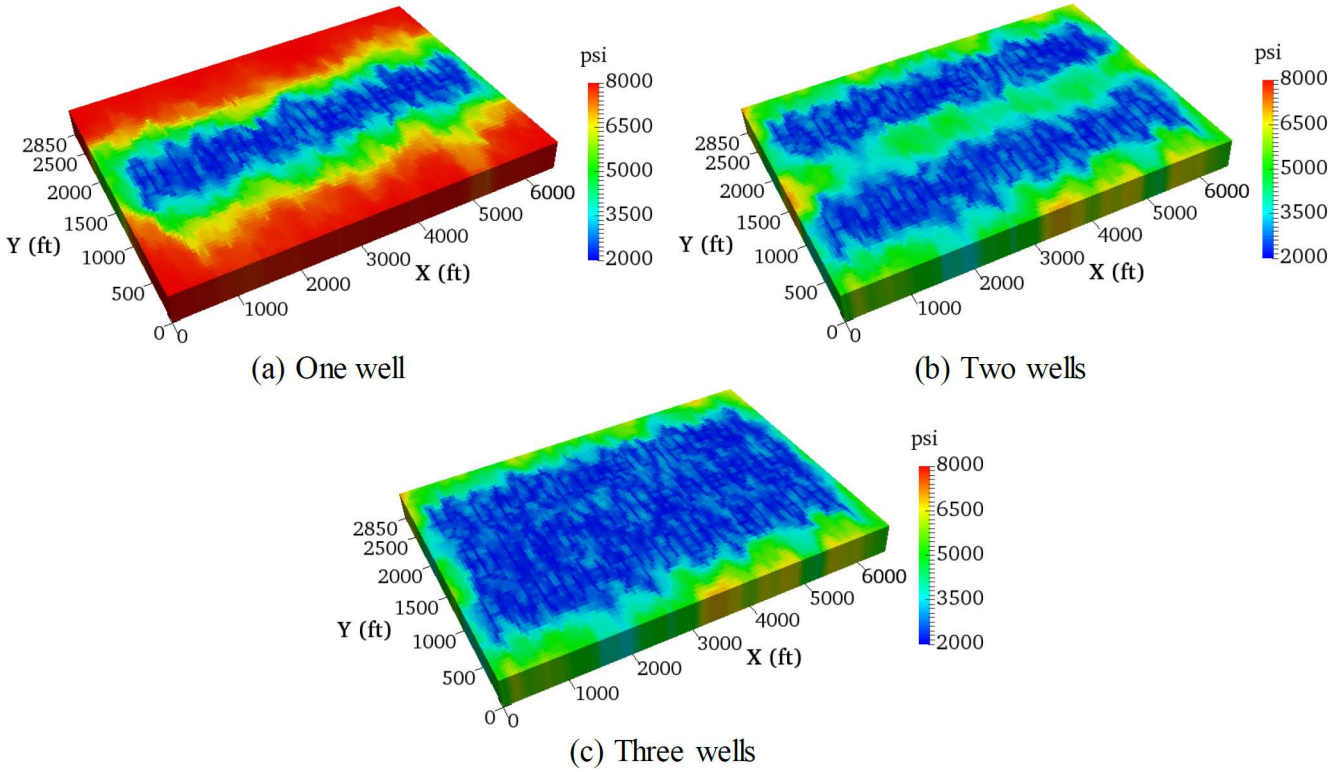

Figure 22—Comparison of pressure distribution between three cases after 1,000 days of production.

Production with some wells shut-in

For the case with three producing wells shown in Fig. 20(c), we also plotted cumulative production if some wells are kept shut-in. Cumulative oil and gas production after 30 years are compared in Fig. 23. Production of the region with only the upper well open is only 66% as compared to production with all three wells open. Production with only the middle well or the lower well produces about 83% as compared to production with all three wells open. The reason for better production performance by the lower wells again is that there is a stronger well-to-well connection between the middle well and the lower well. The pressure drawdown after 30 years of production (Fig. 24) shows reservoir depletion being the largest for production with all three wells open, and least with only the upper well open. Producing via either only the middle or only the lower well shows spatial depletion of the reservoir with similar areas.

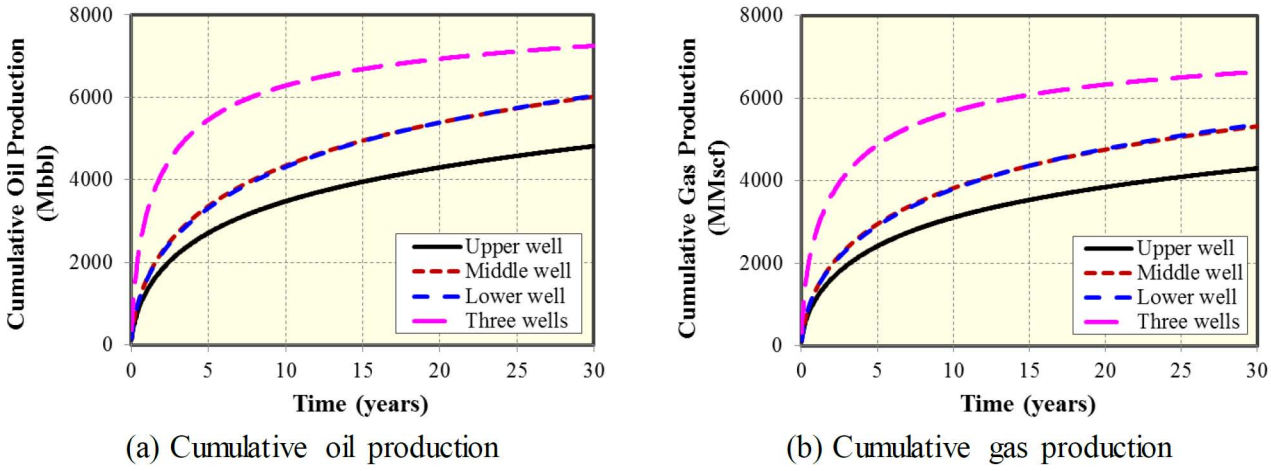

Figure 23—Comparison of well performance between only opening one well while shutting in the other two wells and opening three wells at 30 years of production.

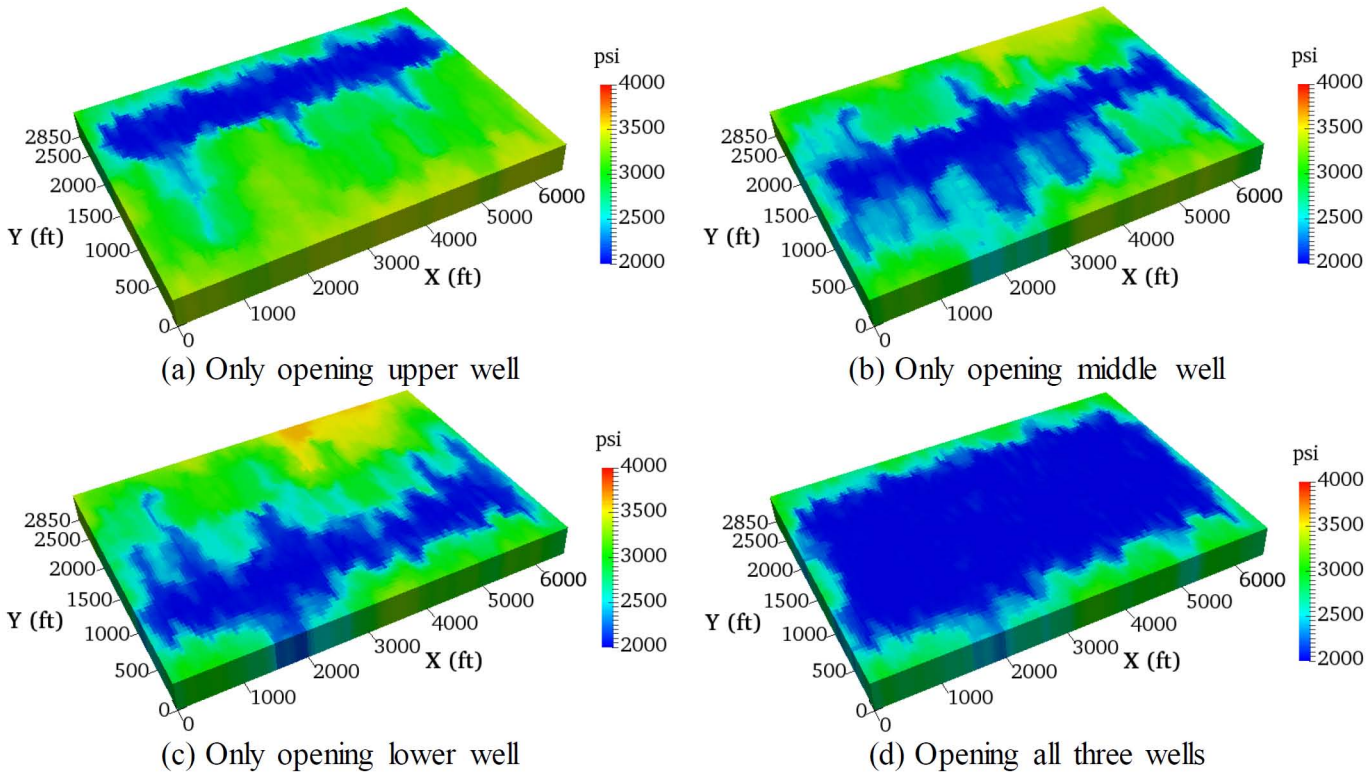

Figure 24—Comparison of pressure distribution between four cases after 30 years of production.

Discussion

Our study focused on quantifying both pressure drawdown and production performance for well interference. A good match of well performance between the proposed model and commercial reservoir simulator is obtained for two horizontal wells with multiple planar hydraulic fractures. The impact on cumulative oil production for all reservoir models in this study is summarized in Tables 4 and 5. First, Table 4 gives the cumulative production summary of 2 wells spaced 700 ft apart for simulations with only planar hydraulic fractures and natural fractures. The cumulative oil production after 1,000 days is highest for 5 hydraulic fracture hits (100 md-ft) and 1,500 natural fractures (1 md-ft) (Table 4, experiment series 4), illustrating that the connecting hydraulic fractures and the natural fracture density significantly affects well productivity. The number of hydraulic fracture hits (Table 4, experiment series 3) and conductivities

of connecting hydraulic fractures (Table 4, experiment series 2) are more sensitive than matrix permeability (Table 4, experiment series 1) to affect well performance.

Table 4—Production summary of 2 wells spaced 700 ft apart with only planar hydraulic fractures and natural fractures.

Numerical experiment series	Cases	Model description		Model design	1,000 days production (Mbbl)	Cumulative production profile
1	Base Case 1	No natural fractures and no hydraulic fracture hits		Fig. 5(a)	**591**	Fig. 6(b)
	Base Case 2	Only natural fractures (1 md-ft)		Fig. 5(b)	**1,101**	
	Base Case 3	Only 5 hydraulic fracture hits (100 md-ft)		Fig. 5(c)	**831**	
	Base Case 4	5 hydraulic fracture hits (100 md-ft) and natural fractures (1 md-ft)		Fig. 5(d)	**1,378**	
2	Base Case 3	Only 5 hydraulic fracture hits with variable conductivities	0.1 md-ft	Fig. 5(c)	**618**	Fig. 8(b)
			1 md-ft		**679**	
			10 md-ft		**831**	
			100 md-ft		**913**	
3	Base Case 3	Only hydraulic fracture hits with varying number of connecting fractures (100 md-ft)	3	Fig. 10(a)	**751**	Fig. 11(b)
			5	Fig. 10(b)	**831**	
			8	Fig. 10(c)	**917**	
			15	Fig. 10(d)	**1,059**	
4	Base Case 4	5 hydraulic fracture hits (100 md-ft) and natural fractures (1 md-ft) with varying natural fracture density	100	Fig. 11(a)	**885**	Fig. 14(b)
			500	Fig. 11(b)	**1,090**	
			1,000	Fig. 11(c)	**1,378**	
			1,500	Fig. 11(d)	**1,670**	

Table 5—Production summary of 3 wells spaced 700 ft apart with non-planar hydraulic fractures and natural fractures.

Numerical experiment series	Cases	Model description	Model design	30 years production (Mbbl)	Cumulative production profile
5	One well	One well in study area	Fig. 20(a)	**3,915**	Fig. 21(a)
	Two wells	Well separation 1400 ft	Fig. 20(b)	**6,932**	
	Three wells	Well separation 700 ft	Fig. 20(c)	**7,248**	
6	Upper well	Only upper well producing other 2 wells shut in	Fig. 20(c)	**4,818**	Fig. 23(a)
	Middle well	Only middle well is producing other 2 wells shut in		**6,022**	
	Lower well	Only lower well is producing other 2 wells shut in		**6,043**	
	Three wells	All three wells producing		**7,248**	

Table 5 provides a cumulative production summary of up to 3 wells spaced 700 ft apart with non-planar hydraulic fractures and natural fractures. Two wells spaced 1,400 ft apart can produce 96% of total production as compared to production by three wells spaced 700 ft (Table 5, experiment series 5). In addition, when production occurs with both the middle and upper wells shut-in, the lower well can produce 83% of total production as compared to three wells open (Table 5, experiment series 6).

It is important to mention that the impacts of natural fractures on well interference were less important than hydraulic fractures in the models of our study because a small conductivity (1 md-ft) was assigned to natural fractures while a higher conductivity (100 md-ft) to hydraulic fractures. Results in the field may be different when naturally fractured reservoirs have higher fracture conductivities than assumed here. Future study will examine the impacts of propped and unpropped natural fractures, as well as natural and hydraulic fractures with varying fracture conductivities. Furthermore, pressure dependent fracture conductivity and matrix permeability can be taken into account.

Although the case studies in this work are mainly focused on shale oil reservoirs, the developed numerical compositional model can also handle well interference in shale gas and gas condensate reservoirs. Furthermore, well interference through fracture hits in shale formation with multiple layers can be accommodated by a 3D expansion of our numerical model.

Conclusions

We developed a numerical compositional model to simulate well performance and pressure response of well interference through complex fracture hits. The model is verified using an independent commercial, numerical reservoir simulator. Different mechanisms for inducing well interference were examined. The impacts of fracture properties on pressure response of well interference were investigated, varying the number of connecting fracture, connecting fracture conductivity, and intensity of natural fractures. Well interference intensity between three wells was separately modelled. The following practical conclusions can be drawn from our synthetic well study:

1. Well spacing remains the most important element in well design for maximizing production. Our reservoir model with 700 ft spacing of 3 wells after 30 years produced only 4% more as compared to two wells spaced by 1,400 ft. We conclude that the 700 ft well spacing with 225 ft hydraulic fracture half-length is a design solution unnecessary closely spaced with a less economic production, because the 4% production gain as compared to 1,400 ft well spacing over 30 years most likely does not justify the extra cost for drilling and completion of the third well (and incurring still more expenses installing the wellhead and separators for that extra well).
2. When tight well-spacing and shut-in tests reveal significant interference between wells occurs, production with only one well open instead of all drilled wells open could be more economic. For example, Fig. 23 shows production with only one well open (and three wells drilled and completed) delivers after 30 years as much as 83% of cumulative production with all three wells open. Producing multiple wells from a single wellhead requires savings on surface facilities must be higher than the revenue cut due to slightly lower cumulative production over a certain time. Additionally, we assume the well life for the single wellhead solution to be longer and ultimate recovery may equal or exceed the three wellhead solution.
3. In order to establish how severe the actual well interference is due to overly close well spacing, well shut-in tests can be used as follows. The rate of pressure decline in the shut-in well after opening an adjacent producer is indicative for the degree of well interference, which in our model is mostly controlled by the number of fracture hits [Fig. 6(a), Fig. 11(a)] and their conductivity [Fig. 8(a)].
4. In order to know, which pair of three well has the largest interference with the middle well, first open the upper well and check the pressure response in the lowermost of the three shut-in wells. Separately, test the pressure response of the uppermost well after shut-in (and after opening of the lower well).

The middle well remains shut-in during the pressure test at all times. The well with the largest pressure decline (either uppermost or lowermost) has the strongest interference with the middle well [e.g., Figs. 19(a) and (b)]. Therefore, if production is decided with only one wellhead and two of the three wells is kept permanently shut-in, the producer needs to be the one well with the largest pressure decline during the well shut-in pressure tests.

5. In our model, the effect of natural fractures on BHP is minor because a relatively low conductivity was assigned (1 md-ft). The effect may be more significant and beneficial for single wellhead production of multiple horizontal wells if the natural fracture conductivity is higher, in which case further modelling is required.

Acknowledgements

The authors would like to acknowledge financial support from Texas A&M Engineering Experiment Station (TEES). Dr. Wei Yu was supported by startup funds from the research group of Dr. Weijermars. We would also like to acknowledge Computer Modeling Group Ltd. for providing the CMG-GEM software for this study.

Nomenclature

EDFM = Embedded discrete fracture model
BHP = Bottomhole pressure
NNCs = Non-neighboring connections
GOR = Gas oil ratio
LGR = Local grid refinement
MMscf = 10^6 standard cubic feet
t = Time
W_i = Accumulation term
$\vec{F}_i$ = Flux term
R_i = Source term
ϕ = Porosity
V_b = Bulk volume
N_p = Number of phases
S = Fluid phase saturation
ξ = Molar density
x = Mole fraction of component in phase
$\vec{u}$ = Phase velocity
$\vec{\vec{k}}$ = Permeability tensor
k_r = Relative permeability
μ = Phase viscosity
D = Depth
γ = Specific gravity
p = Pressure
q = Molar injection or production rate
N_c = Number of hydrocarbon components
V_P^0 = Pore volume at reference pressure
$\vec{V}_t$ = Partial molar volume
p_{cj} = Capillary between phase j and reference phase
K_{NNC} = Permeability associated with the connection

A_{NNC} = Contact area between the NNC pair
d_{NNC} = Distance between the NNC pair
w_f = Fracture aperture
k_f = Fracture permeability
L = Length of the fracture segment

SI Metric Conversion Factors

ft	×	3.048	e-01	=	m
ft^3	×	2.832	e-02	=	m^3
cp	×	1.0	e-03	=	Pa·s
psi	×	6.895	e+00	=	kPa
md	×	1e-15	e+00	=	m^2

References

Ajani, A., and Kelkar, M. 2012. Interference Study in Shale Plays. Presented at the SPE Hydraulic Fracturing Technology Conference, The Woodlands, Texas, 6-8 February. SPE-151045-MS.

Awada, A., Santo, M., and Lougheed, D. 2016. Is That Interference? A Work Flow for Identifying and Analyzing Communication through Hydraulic Fractures in a Multi-Well Pad. *SPE J.* **21** (5): 1554-1566. SPE-178509-PA.

Cavalcante Filho, J. S. A., Shakiba, M., Moinfar, A., and Sepehrnoori, K. 2015. Implementation of a Preprocessor for Embedded Discrete Fracture Modeling in an IMPEC Compositional Reservoir Simulator. Presented at the SPE Reservoir Simulation Symposium, Houston, Texas, 23-25 February. SPE-173289-MS.

Cipolla, C. L., and Wallace, J. 2014. Stimulated Reservoir Volume: a Misapplied Concept? Presented at the SPE Hydraulic Fracturing Technology Conference, The Woodlands, Texas, 4-6 February. SPE-168596-MS.

CMG. 2012. *GEM User's Guide*. Computer Modeling Group Ltd.

King, G. E., and Valencia, R. L. 2016. Well Integrity for Fracturing and Re-Fracturing: What is Needed and Why? Presented at the SPE Hydraulic Fracturing Technology Conference, The Woodlands, Texas, 9-11 February. SPE-179120-MS.

Kurtoglu, B., and Salman, A. 2015. How to Utilize Hydraulic Fracture Interference to Improve Unconventional Development? Presented at the International Petroleum Exhibition and Conference, Abu Dhabi, UAE, 9-12 November. SPE-177953-MS.

Lake, L. W. 1989. *Enhanced Oil Recovery*. Englewood Cliffs, New Jersey: Prentice Hall.

Lawal, H., Jackson, G., Abolo, N., and Flores, C. 2013. A Novel Approach to Modeling and Forecasting Frac Hits in Shale Gas Wells. Presented at the EAGE Annual Conference & Exhibition, London, United Kingdom, 10-13 June. SPE-164898-MS.

Lindner, P. and Bello, H. 2015. Eagle Ford Well Spacing: A Methodology to Integrate, Analyze, and Visualize Multisource Data in Solving a Complex Value-Fouced Problem. Presented at the Unconventional Resources Technology Conference, San Antonio, Texas, 20-22 July. URTEC-2174709-MS.

Lohrenz, J., Bray, B. G., and Clark, C. R. 1964. Calculating Viscosities of Reservoir Fluids from Their Compositions. *Journal of Petroleum Technology* **16** (10): 1171-1176. SPE-915-PA.

Malpani, R., Sinha, S., Charry, L., Sinosic, B., Clark, B., and Gakhar, K. 2015. Improving Hydrocarbon Recovery of Horizontal Shale Wells through Refracturing. Presented at the SPE/CSUR Unconventional Resources Conference, Calgary, Alberta, Canada, 20-22 October. SPE-175920-MS.

Marongiu-Porcu, M., Lee, D., Shan, D., and Morales, A. 2016. Advanced Modeling of Interwell-Fracturing Interference: An Eagle Ford Shale-Oil Study. *SPE J.* **21** (5): 1567-1582. SPE-174902-PA.

Mehra, R. K., Heidemann, R. A., and Aziz, K. 1983. An Accelerated Successive Substitution Algorithm. *The Canadian Journal of Chemical Engineeering* **61** (4): 590-596.

Moinfar, A., Varavei, A., Sepehrnoori, K., and Johns, R. T. 2014. Development of an Efficient Embedded Discrete Fracture Model for 3D Compositional Reservoir Simulation in Fractured Reservoirs. *SPE J.* **19** (2): 289-303. SPE-154246-PA.

Morales, A., Zhang, K., Gakhar, K., Porcu, M. M., Lee, D., Shan, D., Malpani, R., Pope, T., Sobernheim, D., and Acock, A. 2016. Advanced Modelinig of Interwell Fracturing Interference: An Eagle Ford Shale Oil Study-Refractuing. Presented at the SPE Hydraulic Fracturing Technology Conference, The Woodlands, Texas, 9-11 February. SPE-179177-MS.

Peng, D. Y., and Robinson, D. B. 1976. A New Two-Constant Equation of State. *Industrial and Engineering Chemistry Fundamentals* **15**: 59-64.

Perschke, D. R., Chang, Y., Pope, G. A., and Sepehrnoori, K. 1989. Comparison Of Phase Behavior Algorithms For An Equation-Of-State Compositional Simulator. *SPE-19443-MS*

Portis, D.H., Bello, H., Murray, M., Barzola, G., Clarke, P., and Canan, K. 2013. Searching for the Optimal Well Spacing in the Eagle Ford Shale: A Practical Tool-Kit. Presented at the Unconventional Resources Technology Conference, Denver, Colorado, 12-14 August. SPE-168810-MS.

Sani, A. M., Podhoretz, S. B., and Chambers, B. D. 2015. The Use of Completion Diagnostics in Haynesville Shale Horizontal Wells to Monitor Fracture Propagation, Well Communication, and Production Impact. Presented at the SPE/CSUR Unconventional Resources Conference, Calgary, Alberta, Canada, 20-22 October. SPE-175917-MS.

Sardinha, C., Petr, C., Lehmann, J., and Pyecroft, J. 2014. Determining Interwell Connectivity and Reservoir Complexity through Frac Pressure Hits and Production Interference Analysis. Presented at the SPE/CSUR Unconventional Resources Conference, Calgary, Alberta, Canada, 30 September-2 October. SPE-171628-MS.

Scott, K. D., Chu, W. C., and Flumerfelt, R. W. 2015. Application of Real-Time Bottom-Hole Pressure to Improve Field Development Strategies in the Midland Basin Wolfcamp Shale. Presented at the Unconventional Resources Technology Conference, San Antonio, Texas, 20-22 July. URTEC-2154675-MS.

Shakiba, M., and Sepehrnoori, K. 2015. Using Embedded Discrete Fracture Model (EDFM) and Microseismic Monitoring Data to Characterize the Complex Hydraulic Fracture Networks. Presented at the SPE Annual Technical Conference and Exhibition, Houston, Texas, 28-30 September. SPE-175142-MS.

Simpson, M. D., Patterson, R., and Wu, K. 2016. Study of Stress Shadow Effects in Eagle Ford Shale: Insight from Field Data Analysis. Presented at the 50th U.S. Rock Mechanics/Geomechanics Symposium, Houston, Texas, 26-29 June.

Wu, K. and Olson, J. E. 2016. Numerical Investigation of Complex Fracture Networks in Naturally Fractured Reservoirs. *SPE Prod & Oper* (in preprint). SPE-173326-PA.

Wu, R., Kresse, O., Weng, X., Cohen, C., and Gu, H. 2012. Modeling of Interaction of Hydraulic Fractures in Complex Fracture Networks. Presented at the SPE Hydraulic Fracture Technology Conference, The Woodlands, Texas, 6-8 February. SPE-152052-MS.

Xu, Y., Cavalcante Filho, J. S. A., Yu, W., and Sepehrnoori, K. 2016. Discrete-Fracture Modeling of Complex Hydraulic-Fracture Geometries in Reservoir Simulators. *SPE Res Eval & Eng* (in preprint). SPE-183647-PA.

Yaich, E., Diaz de Souza, O. C., Foster, R. A. 2014. A Methodology to Quantify the Impact of Well Interference and Optimize Well Spacing in the Marcellus Shale. Presented at SPE/CSUR Unconventional Resources Conference, Calgary, Alberta, Canada, 30 September-2 October. SPE-171578-MS.

Yu, W., Sepehrnoori, K., and Patzek, T. W. 2016. Modeling Gas Adsorption in Marcellus Shale with Langmuir and BET Isotherms. *SPE J.* **21** (2): 589-600. SPE-170801-PA.

Yu, W., Wu, K., Zuo, L., Tan, X., and Weijermars, R. 2016. Physical Models for Inter-Well Interference in Shale Reservoirs: Relative Impacts of Fracture Hits and Matrix Permeability. Presented at the Unconventinoal Resources Technology Conference, San Antonio, Texas, USA, 1-3 August. URTEC-2457663-MS.

Zuloaga-Molero, P., Yu, W., Xu, Y., Sepehrnoori, K., and Li, B. 2016. Simulation Study of CO_2-EOR in Tight Oil Reservoirs with Complex Fracture Geometries. *Scientific Reports* **6**: 33445.